Published in final edited form as:
Clin Genitourin Cancer. 2015 February ; 13(1): e7–e17. doi:10.1016/j.clgc.2014.07.001.

Comparison of NaF and FDG PET/CT for assessment of treatment response in castrate-resistant prostate cancers with osseous metastases

Urban Simoncic[1,2,5], **Scott Perlman**[3,6], **Glenn Liu**[4,6], **Mary Jane Staab**[6], **Jane Straus**[6], and **Robert Jeraj**[1,2,3,5,6]

[1]Jozef Stefan Institute, Jamova 39, SI–1000 Ljubljana, Slovenia

[2]Department of Medical Physics, University of Wisconsin – Madison, 1111 Highland Avenue, Madison, WI 53705–2275, USA

[3]Department of Radiology, University of Wisconsin – Madison, 1111 Highland Avenue, Madison, WI 53705–2275, USA

[4]Genitourinary Oncology Research Program, University of Wisconsin Carbone Cancer Center, 600 Highland Avenue, Madison, WI 53792

[5]The Centre of Excellence for Biosensors, Instrumentation and Process Control – COBIK, Tovarniska 26, SI-5270 Ajdovscina, Slovenia

[6]University of Wisconsin Carbone Cancer Center, University of Wisconsin, 1111 Highland Avenue, Madison, WI 53705–2275, USA

Abstract

Background—Assessment of skeletal metastases response to therapy is highly relevant, but unresolved clinical problem. The main goal of this work was to compare pharmacodynamic responses to therapy assessed with NaF and FDG PET/CT.

Materials and Methods—Prostate cancer patients with known osseous metastases were treated with Zibotentan (ZD4054) and imaged with combined dynamic NaF/FDG PET/CT prior to therapy (Baseline), after 4 weeks of therapy (Week 4) and after 2 weeks of treatment break (Week 6). Kinetic analysis allowed comparison of voxel-based tracer uptake rate parameter K_i, vasculature parameters K_1 (measuring perfusion/permeability) and V_b (measuring vasculature fraction in the tissue) together with standardized uptake values (SUVs).

Results—Correlations were high for the NaF and FDG peak uptake parameters (K_i and SUV correlations ranged from 0.57 to 0.88) and for vasculature parameters (K_1 and V_b correlations

First and corresponding author: Urban Simoncic Institute Jozef Stefan Jamova 39 SI-1000 Ljubljana Slovenia urban.simoncic@ijs.si.

Conflict of Interest Notification
There are no conflicts of interests.

ranged from 0.61 to 0.81). Correlation between the NaF and FDG Week 4 K_i responses was low (ρ=0.35, p=0.084), but higher for NaF and FDG Week 6 K_i responses (ρ=0.72, p<0.0001). Correlations for vasculature responses were always low (ρ<0.35). NaF and FDG uptakes in the osseous metastases were spatially dislocated, with overlap in the range from 0% to 80%.

Conclusions—These results showed that late NaF and FDG uptake responses are consistently correlated, but earlier uptake responses and all vasculature responses can be unrelated. This study also proved that FDG and NaF uptakes are spatially dislocated. Although treatment responses assessed with NaF and FDG may be correlated, using both tracers provides additional information.

Keywords

NaF PET/CT imaging; FDG PET/CT imaging; prostate cancer; skeletal metastases; therapy response assessment

Introduction

Prostate cancer is the most common solid malignancy in men and it is second in cancer-related mortality[1]. While androgen-deprivation therapy is the mainstay of treatment in those with advanced disease, eventually all patients develop castrate-resistant prostate cancer (CRPC)[2]. The development of osseous metastases is the principal site of prostate cancer spread[3]. Detection and staging of skeletal metastases is most often performed with the bone scintigraphy (BS), but positron emission tomography (PET), aided with computed tomography (CT), can provide greater sensitivity and spatial information than BS. Magnetic resonance imaging (MRI) and X-ray are often used in case of equivocal findings. CT, MRI and PET are used also to detect soft tissue metastases. BS is an appropriate imaging modality also to evaluate new osseous lesions as an indication of disease progression, but there is no good way to assess the response to treatment in osseous metastases. In the absence of quantitative treatment response imaging biomarker, the Prostate Cancer Clinical Trials Working Group currently advocates the use of a time to event, such as radiographic progression-free survival, as a preferred endpoint for early drug development in prostate cancer[4]. It is anticipated that out of many imaging modalities, which have been shown to be able to detect metastases arising from CRPC, some have the potential to be used for quantitative treatment response assessment[5].

PET/CT remains the most promising imaging modality. The most commonly used tracer is 2-[^{18}F]-fluoro-2-deoxy-D-glucose (FDG), which is a surrogate for glucose metabolism[6]. The key advantage of FDG PET/CT is the ability to obtain metabolic activity information, and thus the potential to gage response to therapy[7]. The FDG PET therapy response assessments in men with osseous metastatic prostate cancer are not always in agreement with composite clinical designations of response, stable disease, or progression[8]. Generally, the FDG avidity is low in treatment naïve prostate cancer, increased in CRPC, and almost always present in docetaxel-refractory prostate cancer[9-10]. All this indicate that the FDG is not ideal for response assessment of prostate cancer osseous metastases especially in earlier disease states.

[^{18}F]NaF (NaF) is another tracer that is gaining popularity in recent years[11]. NaF has high sensitivity in detecting osseous metastases, with its uptake representing both the increased blood flow and bone turnover characteristic of malignant lesions in bone[12]. The NaF PET therapy response assessments in men with osseous metastases from CRPC that were treated with radium-223 (^{223}Ra)-chloride (Alpharadin) showed notable agreement with prostate-specific antigen (PSA) responses and alkaline phosphatase (ALP) activities[13]. Due to high sensitivity of NaF in detecting osseous metastases and successful NaF PET therapy response assessments in men with osseous metastases from CRPC the quantitative NaF PET imaging has a great potential to become imaging biomarker for monitoring treatment response in osseous metastases originating from CRPC.

The diagnostic comparison between NaF PET/CT and FDG PET/CT has shown the superiority of NaF PET/CT over FDG PET/CT and bone scans[14]. The combination of NaF and FDG PET/CT has been assessed preclinically, and found to improve osseous metastases detection rates by the dual ability to characterize both lytic and blastic osseous metastases[15]. Early clinical experience with the combined tracer cocktail proved this approach to be feasible[16] and thus opens the potential for its use in both diagnostics as well as response assessments. Several clinical studies have found increased sensitivity of combined NaF/FDG PET/CT for detection of osseous lesions when compared with separate NaF PET/CT and FDG PET/CT[17-21]. No previous studies have focused on differences in concurrent NaF PET and FDG PET therapy response assessment for osseous metastases and spatial differences in NaF and FDG uptake into osseous metastases, which is the main goal of this article.

Methods and materials

Study Design

The purpose of described clinical study was to determine the pharmacodynamic effects of Zibotetan (ZD4054) with the various imaging tools (CT, BS, MRI, NaF/FDG PET) in order to evaluate the potential of these imaging tools to assess early treatment response in bone metastases, understanding that each imaging tracer/modality provides complementary information. Despite using various imaging tools in the clinical study, this article focuses into results from NaF/FDG PET imaging. The rationale to assess both FDG and NaF was several folds: 1) NaF is one of the most sensitive modalities to assess osteobloastic metastases, however, its sensitivity in osteolytic metastasis is low. 2) NaF PET indirectly assesses change in cancer burden in bone as its uptake reflects a stromal response to prostate cancer. This is in contrast to FDG, which more directly reflects the tumor compartment. 3) FDG is not ideal for use in prostate cancer due variable avidity.

Study was designed to enroll ten patients with progressive, metastatic CRPC with known osseous metastases. All patients were treated with ZD4054 at 10 mg PO daily, repeated in four week cycles (1 cycle = 28 days), except for the first cycle that was a six week cycle. All patients initially received a diagnostic CT and bone scan, followed by NaF/FDG PET/CT and MRI imaging at Baseline (scan #1), and then again after 4 weeks (scan #2) of ZD4054 exposure. Subsequently, ZD4054 was held for 2 weeks followed by the final NaF/FDG PET/CT and MRI acquisition (scan #3). After the final PET and MRI were obtained, patients resumed ZD4054 and were assessed for safety prior to each new cycle of therapy.

Disease evaluation assessments with bone scans (and CT if soft-tissue lesions found at baseline, or as clinically indicated) were conducted after cycle #3, and repeated after every third cycle (sooner if clinically indicated). Therapy continued until radiographical/clinical disease progression or unacceptable toxicity. PCWG2 criteria were used to define bone scan progression, while PSA levels were not considered as valid marker for disease progression.

It was acknowledged that observed changes in the imaging metrics could be a result of the therapy effect or a natural evolution of the prostate cancer bone metastasis. A short therapy break allowing for complete drug washout and repeated imaging was imposed to determine the cause of changes in imaging metrics. The assumption was that a change in imaging metrics from Baseline to Week 4 (on therapy) would be most consistent with a therapy effect if the repeated imaging at Week 6 (drug break) showed a change back towards Baseline during the therapy break. In contrast to that, from a change from Baseline to Week 4 (on therapy) that persisted at Week 6 (drug break) one could not be able to assume that the imaging change was due to the treatment effect. The two week drug washout was based on the half-life of ZD4054, assuring complete drug washout before the Week 6 imaging.

Patient Selection

This study enrolled male patients older than 18 years, with histologically proven adenocarcinoma of prostate and presence of radiographic osseous metastasis. At least one clinically/radiographically identified prostate metastasis in the vertebral body, pelvis or other bone had to be amenable to serial imaging using PET/CT and MRI imaging. Preference was given to subjects with multiple lesions that can be imaged in one image acquisition session to obtain maximal information. Patients were selected for enrolment based on appropriate osseous lesions appropriate for pharmacodynamic imaging with planned PET/CT and MRI. Other key inclusion criteria included the following: evidence of progressive disease as evident by either radiographic progression (e.g., new lesions on bone scan or new/enlarging lesions on CT scan) or a rising PSA within four weeks prior to registration (i.e., two subsequent rises in PSA measurement, each separated from the previous by a minimum of two weeks), and castrate-resistant disease. Patients had adequate bone marrow function (WBC above 4000/mm^3, Granulocytes above 2000/mm^3 and Platelet count above 100,000/mm^3). Exclusion criteria included Bilirubin above 1.5 mg/dl, SGPT (ALT) above two times the institutional upper limit of normal, Creatinine above 1.5 mg/dL AND a calculated creatinine clearance below 50 ml/min, and ECOG performance status >2.

Prior use of bisphosphonates was allowed only if started at least twelve or more weeks prior to registration (were able to continue current dose/schedule while on study). Initiation of new bisphosphonates therapy were not permitted while on study unless clinically indicated (e.g., to treat hypercalcemia of malignancy). No concurrent use of estrogen, or estrogen-like agents (i.e. PC-SPES, Saw Palmetto, or other herbal products which may contain phytoestrogens), or any other hormonal therapy (including megastrol acetate, finasteride, and systemic corticosteroids) were allowed. Prior use of these agents had to be discontinued at least four weeks prior to enrollment. Patients that were previously treated with flutamide (Eulexin), nilutamide (Nilandron), or bicalutamide (Casodex) had to have discontinued flutamide at least four weeks prior to registration with continued evidence of progressive

disease (flutamide), and at least six weeks prior to registration with evidence of progressive disease (bicalutamide or nilutamide). Disease progression following anti-androgen withdrawal had to show evidence of progressive metastatic disease or rising PSA after the required four or six week period compared to prior to that period.

Treatment continued until one of the following criteria was met: disease progression (clinical or radiographical), greater than two week delay of treatment for treatment-related toxicity, intercurrent illness that prevents further administration of treatment, unacceptable adverse event(s), patient decided to withdraw from the study, general or specific changes in the patient's condition render the patient unacceptable for further treatment in the judgment of the investigator.

All patients signed informed consent documents approved by the Institutional Review Board at the University of Wisconsin prior to any study-related procedures.

Treatment

ZD4054 (Zibotentan, AstraZeneca) is a selective Endothelin receptor A antagonist that was an investigational agent in Phase III trials for men with metastatic CRPC. ZD4054 was administered on an outpatient basis at the starting dose of 10 mg PO continuous daily basis. Cycle #1 was six weeks in duration and was dosed as follows: ZD4054 was administered in cycle #1 from days 1 to 28 (+/− 2 days), which was followed by stoppage of ZD4054 for 14 days (+/− 2 days). The purpose for this dosing schedule was to allow pharmacodynamic imaging to be conducted during and after ZD4054 exposure. All subsequent cycles of therapy were four weeks in duration.

NaF/FDG PET/CT imaging

Patients received a combined NaF/FDG PET/CT scans before the therapy (Baseline), at peak drug exposure (Week 4), and at maximal drug washout (Week 6). To minimize uncertainties inherent in PET imaging, strict imaging procedures were followed, including employing optimized and standardized image acquisition and reconstruction protocols. At the beginning of each imaging session, a high-quality CT scan was obtained on the combined PET/CT scanner. The CT scan served for attenuation correction calculations, better PET/CT image registration and it also enabled better delineation of the patient anatomy, which was important when comparing different scans. Patients were injected 120 MBq (range 107 MBq to 166 MBq) of NaF while lying on the scanner table. A 30 min dynamic PET acquisition started with the injection of NaF. The dynamic PET image had 21 time frames with the following durations: 8×15 s, 4×30 s, 6×1 min, 2×5 min and 1×10 min. A scan region of approximately 15 cm was identified by a nuclear medicine physician based on the diagnostic bone scan, with the aim to include the highest suspected density of lesions. If applicable, the region that allowed at least a partial heart view was selected. A static whole body scan initiated approximately 50 minutes after the injection of NaF. A static scan of 3 min over the same position as the NaF PET/CT dynamic scan was initiated at 100 min post-injection (range 78 min to 113 min) to provide the baseline for subsequent FDG scan. The FDG with activity of 240 MBq (range 218 MBq to 263 MBq) was injected after the end of static scan. The second dynamic scan had 23 time frames with the following durations: 8×15 s, 4×30 s,

6×1 min, 2×5 min, 2×10 min and 1×5 min. The sequence of tracer injections and image acquisitions is in Figure 1.

All the scans were acquired in a 3D acquisition mode. A 3D ordered-subsets expectation maximization (OSEM) was used for image reconstruction. The OSEM reconstruction matrix was 256×256 with the 3 mm post filtering with 2 iterations and 35 subsets. All scans were performed on the Discovery VCT PET/CT scanner (General Electric). The data were collected in the Wisconsin Institutes for Medical Research at the University of Wisconsin - Madison.

PET/CT image analysis

Because two PET tracers with comparable half-lives were concurrently investigated, the analysis was, unfortunately, restricted to the dynamic field of view (FOV) as the scanner needed to acquire time-dependent dynamic data to resolve contributions from each tracer. Second PET scan was whole-body instead of one time frame for possible NaF PET/CT evaluation of lesions outside the FOV of dynamic PET. However, as the whole-body FDG PET/CT scans were not available (FDG PET/CT whole body scan would have been confounded with the NaF PET/CT uptake, which would not be resolvable without dynamic acquisition) we were limited to the NaF/FDG comparison only within the dynamic FOV. Because ZD4054 has both vascular as well as osteoblastic effects, the use of uptake rate (K_i, *SUV*) and vascular parameters (K_1, V_b) for both tracers was of high interest in order to assess the tumor stromal compartment.

The first dynamic PET scan, whole-body PET scan, static 3 min PET scan and second dynamic PET scan were registered rigidly, based on the CT data, in order to form a combined dynamic NaF/FDG PET/CT image. The NaF part of the image (first dynamic scan, whole body scan and static 3 min scan) was analyzed for kinetics using the two-tissue compartment with four kinetic parameters and vasculature fraction[22]. Additionally, the delay between the input function and tissue time activity curve (TAC) was imposed as a free parameter. The blood TAC, used as an input function, was obtained by placing the ROI on large vasculature structure (aortic arch or abdominal aorta), taking the average TAC over this region and scaling with a plasma-to-whole-blood ratio of 1.2[22-23]. The vasculature structure was segmented on one of the early time frames, where the blood activity was clearly visible. Great attention was paid to segment the same part (size and location) for the Baseline, Week 4 and Week 6 imaging sessions, which assured that any possible error due to partial volume effect was roughly the same for all the sessions and canceled out when response was calculated. The NaF kinetic analysis results were used to extrapolate the NaF part of combined NaF/FDG PET image. Extrapolated NaF part was subtracted from the combined NaF/FDG PET image, producing the FDG dynamic PET image. The FDG dynamic PET image was analyzed for kinetics using two-tissue compartment with three kinetic parameters[24]. Additionally, the vasculature fraction and delay between the input function and tissue TAC were imposed as free parameters. The blood TAC, used as an input function, was obtained in the same way as for the NaF kinetic analysis, except that the plasma-to-whole-blood ratio was assumed to be 1[25]. The kinetic analysis was done on a voxel basis, which resulted in parametric images. The macroparameter $K_i = K_1k_3/(k_2+k_3)$

that accounts for the tracer influx rate to the cell was calculated from the microparameters obtained with kinetic analysis. The NaF and FDG Standardized Uptake Values (SUV) at 60 min post-injection were calculated on a voxel basis using the compartmental model, input functions and estimated kinetic parameters.

Both, the CT data (anatomical information) and PET data (functional/molecular information) were used to identify metastases. All the visible metastases were included in the analysis. Uptake patterns of NaF and FDG were compared visually. Lesions were segmented on K_i parametric images by a two-step process: in the first step all the suspicious regions were segmented. In this step a single segmentation for NaF and FDG parametric images for particular imaging session was created. In the second step the region with NaF or FDG K_i value at least 50% of the maximum in the segmentation from the first step was segmented. In this step separate segmentations for NaF and FDG parametric images were created.

Spatial concordance of FDG and NaF uptake was assessed by the Jaccard index, evaluated on the FDG and NaF segmentations. The Jaccard index is evaluated as a ratio between the size of the overlapped region and the size of the combined region. The value of 0 means no overlapping and the value of 1 means complete overlap.

NaF and FDG K_i responses were evaluated with peak values obtained from K_i parametric images. Three responses were considered: Week 4 response, Week 6 response and change from Week 4 to Week 6. All responses were evaluated as a difference, normalized to the Baseline value. NaF and FDG K_1, V_b and *SUV* responses were evaluated as well. Responses were compared with the average values, correlation plots and correlation coefficients.

The data was analyzed by the Image Analysis Center (IMAC) at the University of Wisconsin. Registration was done with Amira software (VSG). All other analysis was done with Matlab (The Mathworks).

Results

Patient characteristics

From June 2010 to May 2011, 6 patients were enrolled at the University of Wisconsin Carbone Cancer Center. No more patients were added to the study because the study was stopped due negative Phase III trial results[26] and decision to not further develop ZD4054. Median age was 68 (range: 57–88). Four patients received prior docetaxel chemotherapy, of which one had both docetaxel and mitoxantrone chemotherapy. No clinical/PSA responses were observed. Median number of cycles received was 2 (range 2-6). Five patients discontinued protocol therapy for clinical progression/physician discretion. One patient withdrew consent. Four patients were imaged in pelvic region and two in lumbar spine region. Up to eight lesions were segmented on each patient with a total of 26 lesions were segmented. Peak vasculature parameters (K_1, V_b), uptake rate parameter K_i and SUV for both tracers and all imaging sessions, averaged over all segmented lesions are in Table 1. Responses for both tracers and all imaging sessions, evaluated through vasculature

parameters (K_1, V_b), uptake rate parameter K_i and SUV, and averaged over all segmented lesions are in Table 2.

Comparison of FDG and NaF uptake parameters and responses

The Baseline NaF and FDG peak SUV's were correlated, but some intrapatient lesion-to-lesion heterogeneity in PET tracers uptake was still noticeable. The Figure 2 shows correlation plots for NaF and FDG peak SUV for all the lesions, for patients with multiple lesions. These plots illustrate the intrapatient NaF/FDG uptake heterogeneity, which is high for some patients; e.g. two lesions in patient #1 have similas NaF SUV (approximately 31) and substantially different FDG SUV (5.3 vs. 7.1), or two lesions in patient #2 having similar FDG SUV (slightly above 5) and NaF SUV either 16.2 or 23.5. Despite this heterogeneity, no single lesion was visible only on the NaF or FDG SUV image.

Correlations of NaF and FDG uptake parameters and responses evaluated through peak values are in Table 3. All uptake parameters were highly correlated on population level. Responses based on uptake rate parameters (K_i, SUV) showed higher correlation on population level than the vasculature parameters (K_1, V_b).

Overall correlation between the NaF and FDG Week 4 K_i responses was moderate ($\rho=0.35$, $p=0.084$), but depended considerably on the patient. For patients #1 and #3, the FDG Week 4 K_i responses were grouped close to zero and they were unrelated or even anti-correlated to corresponding NaF responses. Correlation between the NaF and FDG Week 6 K_i responses was high ($\rho=0.72$, $p<0.0001$), with linear relation visible for all the patients. The NaF and FDG K_i changes from Week 4 to Week 6 were anti-correlated ($\rho=-0.49$, $p=0.011$). High correlations were observed also between some other K_i responses, especially between the NaF Week 4 K_i responses and the FDG Week 6 K_i responses ($\rho=0.80$, $p<0.0001$), but also between the NaF Week 6 K_i responses and the FDG Week 4 K_i responses ($\rho=0.73$, $p<0.0001$) and between the NaF Week 4 K_i responses and FDG K_i changes from Week 4 to Week 6 ($\rho=0.69$, $p=0.0001$). On the other hand, correlations between the Week 4 K_i responses and Week 6 $K_i$responses for the same tracer were lower; $\rho=0.52$ ($p=0.0064$) and $\rho=0.67$ ($p=0.0002$) for the NaF and FDG, respectively. Correlations between the Week 4 K_i responses and K_i changes from Week 4 to Week 6 for the same tracer were even lower; $\rho=-0.44$ ($p=0.025$) and $\rho=-0.17$ ($p=0.41$) for the NaF and FDG, respectively.

Figure 3 shows the correlation plots of equivalent NaF and FDG K_i responses. The correlation plot of NaF Week 4 K_i responses versus FDG Week 4 K_i responses (Figure 3a) shows a clear linear relation for patient #2, while it appears that FDG Week 4 K_i responses were unrelated to NaF Week 4 $K_i$responses for patient #3 and even slightly anti-correlated for patient #1. Week 6 K_i responses (Figure 3b) were more correlated, although the correlation plot is “broad”.

The correlation plot of NaF Week 4 K_i responses versus FDG Week 6 K_i responses (Figure 4a) has most distinct linear relation, but two clear outliers – one is patient #4 and another is one of the metastasis from patient #2. Visual evaluation of NaF Week 6 K_i responses versus Week 4 FDG K_i responses (Figure 4b) revealed a clear linear relation for patient #2 and #6, while patients #1 and #3 showed a cloud of points on correlation plot, and patients #4 and #5

are indefinite due to only one point. The NaF Week 4 K_i responses versus FDG K_i changes from Week 4 to Week 6 (Figure 4c) showed a clear linear relation for patients #1 and most lesions of patients #2 and #3, while there were some outliers for patients #2, #3 and #6.

Spatial concordance of NaF and FDG uptake

Spatial concordance of NaF and FDG uptake varied by the case and by the imaging session.

Figure 5 shows an example of NaF, FDG and combined K_i parametric images, where the areas of high NaF and high FDG uptakes were notably dislocated, especially at the Baseline. On contrary to that, in Figure 6, the NaF and FDG uptakes at the Baseline almost coincided.

Concordance of NaF and FDG uptake was measured by the Jaccard index, calculated on the segmentations done on the NaF and FDG K_i parametric images. Figure 7 shows the concordance of NaF and FDG segmentations for all the investigated metastases through the course of therapy. Average spatial concordance of NaF and FDG uptake decreased while on therapy and increased during the treatment break. Changes were not significant and the trend was not consistent for all the lesions.

Discussion

Correlations between the Week 4 K_i responses and Week 6 K_i responses for the same tracer were low and anticorrelations between the Week 4 K_i responses and K_i changes from Week 4 to Week 6 for the same tracer were even lower in absolute value. However, at least signum of those correlations were as expected. Therefore, it is not clear to what degree the changes in NaF or FDG uptakes through the therapy are because of natural evolution of disease, and to what degree due to the treatment effect. Obviously, it would be interesting to correlate the PET responses with a commonly used clinical markers like the ammount of PSA increase. Unfortunately in the development of ZD4054, PSA changes were not reflective of clinical benefit as this class of drug was observed to have increases in PSA despite decreases in soft-tissue tumor lesions.

However, some other significant correlations were observed, which could indicate some inter-relations between the values or changes in the NaF and FDG uptakes through the therapy, and potentially be helpful when designing future clinical studies. Significant correlations between NaF and FDG uptake rates and responses, especially the K_i responses were observed. Overall correlation between the NaF and FDG Week 4 K_i responses was moderate, but depended considerably on the patient. Especially for patients #1 and #3, the FDG Week 4 K_i responses were grouped close to zero and they were unrelated or even anti-correlated to the corresponding NaF K_i responses. Correlation between the NaF and FDG Week 6 K_i responses was high for all patients. High correlations were observed also between some non-equivalent responses, especially between the NaF Week 4 K_i responses and the FDG Week 6 K_i responses, where also the correlation plot showed distinct linear relation, although with two outliers. Correlation between the NaF Week 6 K_i responses and FDG Week 4 K_i responses was also high, but responses for patients #1 and #3 by themselves did not show any correlation. In addition, differences in the average NaF and FDG responses, evaluated through the uptake metrics (K_i, *SUV*), were much lower than the standard

deviations for those responses. All these results indicate that NaF and FDG uptake rate responses over the whole chemotherapy cycle were related, while earlier responses were related for some patients, but unrelated for others because the FDG was not yet stabilized for those patients. It should be noted that these findings apply to tumor phentoypes with predominantly osteoblastic bone metastases and would need to be assessed separately for other cancer phenotypes with predominantly osteolytic or mixed-type bone metastases.

K_i responses in different lesions of the same patient were heterogeneous. For example the lesion #6 in patient #2 had the lowest Baseline FDG uptake and the highest FDG Week 6 uptake amongst all the lesions in the patient. This lesion was one of the two outliers in Figure 4a. Another outlier in this correlation plot was the only lesion in patient #4, which had unusually high FDG Baseline (the highest amongst all the patients) and one of the lowest FDG Week 6 uptake. These outliers showed that for some lesions the responses can be different when estimated by NaF or FDG, which was not unexpected as it is known that diagnostic NaF or FDG PET image may not show all the lesions because the uptake of the tracer is not high enough, compared to the background[16]. Lesions with very low Baseline uptake have high relative increase even if the absolute increase is not that high.

Interestingly, also the vasculature parameters obtained through the NaF and FDG kinetic analysis showed higher correlation than the NaF and FDG uptake rates. On the other hand, the vasculature responses evaluated from the vasculature parameters obtained through the NaF and FDG kinetic analysis showed low correlation, and also differences in the average NaF and FDG responses, evaluated through the vasculature parameters (K_1, V_b) were higher (albeit within the standard deviations) than differences in the average NaF and FDG responses obtained through the uptake metrics (K_i, *SUV*). That might be because the NaF and FDG vasculature parameters measure the same quantity. Imperfect correlations between those parameters and different average values are because the NaF and FDG are different molecules and membrane permeability for those molecules may be different, and because the kinetic analysis errors, which add up when responses are evaluated.

As the imperfect population correlations between the NaF and FDG uptake rate parameters were observed, also the spatially dislocated NaF and FDG uptake into the osseous metastases was observed. Dislocation of NaF and FDG uptake varied by patient/lesion and by imaging session. Lesions with up to 80% overlap between the segmentations based on NaF and FDG were found, as well as lesions with no overlap. There was no significant change in overlap during the therapy. The observed spatially dislocated NaF and FDG uptake into osseous metastases was expected based on the fact that the FDG images tumor and stroma, while the NaF images only the stroma. Although it was expected, this study enabled for the first time to observe spatially dislocated uptake of NaF and FDG in vivo. Incomplete overlaps between the segmentations based on NaF and FDG can be explained by spatial dislocation between the NaF and FDG uptake into the osseous metastases. However, Jaccard indices should be viewed with caution as different overlaps could also be caused by different segmentation sizes, which were affected by noise in maximal K_i value and background uptake.

Although this study showed that PET-based treatment responses over the whole chemotherapy cycle are similar if estimated by NaF or FDG uptake, using both tracers might still be beneficial. One reason is to improve detection/diagnosis, as some lesions might have unusually low uptake on Baseline PET image. Lesions with unusually low Baseline uptake usually have high relative increase of uptake. Another reason for using both tracers is the possibility of uptake flares[27-28]. The ZD4054 treatment was not particularly effective and therefore also the uptake flare is not expected, but with other treatments or different clinical cases the uptake flares are possible. The uptake flare may be for one tracer only, so another tracer may give useful information in that case. Of course, imaging with both tracers does not need to be done concurrently, following the protocol presented here, but it can be done at two separate days. The protocol for concurrent NaF/FDG PET/CT was applied here because we assessed differences in NaF and FDG PET/CT, so we wanted to exclude as many uncertainties as we could.

While this study included only six patients with one particular (blastic) type of osseous metastases originating from one particular cancer (CRPC), some results would likely be similar for any blastic metastases. The NaF and FDG uptakes would likely be spatially dislocated. Spatially dislocated NaF and FDG uptake into osseous metastases put on a question the process of metastases segmentation that relies on the PET/CT, and all the uptake metrics that are sensitive to segmentation (e.g. mean and total uptake). Segmentations based on the NaF PET/CT and FDG PET/CT are not the same and at most one, but probably none really cover the entire metastasis. Therefore, maximal or peak value might be more relevant. Spatial dislocation of NaF and FDG uptake into osseous metastases has even more interesting consequences for possible PET/CT imaging with the cocktail of NaF and FDG. Providing that the NaF and FDG contributions to the PET signal are roughly the same, the metastases segmented on NaF/FDG PET/CT would likely to be bigger, with the total SUV being the same. Therefore, the mean, peak and maximum SUV's would be lower. It is uncertain whether the maximal and peak values are determined mainly by the NaF or FDG uptake, but they are likely not contributed by both tracers in similar proportions.

This study focused on the combined NaF and FDG PET/CT imaging of prostate cancer osseous metastases. The NaF and FDG are two promising tracers for imaging of osseous metastases, but several other promising PET tracers exists, including ^{11}C-labeled or ^{18}F-labeled choline, ^{11}C-labeled or ^{18}F-labeled acetate and ^{68}Ga-labeled PSMA. In addition, MRI techniques for imaging of osseous metastases of prostate cancer also show some potential[5]. While this study found that NaF and FDG responses are highly correlated under some circumstances and the benefit of using both tracers is limited, that might not be the case for combinations with different tracers.

Conclusion

Responses based on NaF and FDG PET/CT imaging at the end of chemotherapy cycle are consistently correlated, with correlation of earlier responses based on NaF and FDG PET/CT imaging being inconsistent. This study has shown that the NaF and FDG uptakes are spatially dislocated and produce different lesion segmentations. These findings led us to the

conclusion that only one tracer can be used for osseous metastases response assessment, but both tracers could provide more information.

Acknowledgment

This study was funded by AstraZeneca. The study was performed under clinical trial registration number NCT01119118 at ClinicalTrials.gov. Additional founding was provided by NIH grant 1R01CA136927, CCSG grant P30CA014520 and Slovenian Research Agency (ARRS). The Centre of Excellence for Biosensors, Instrumentation and Process Control is an operation financed by the European Union, European Regional Development Fund and Republic of Slovenia, Ministry of Higher Education, Science and Technology. The authors wish to thank the UW PET program for conducting and overseeing PET scans.

References

1. Siegel R, Naishadham D, Jemal A. Cancer statistics, 2013. CA Cancer J Clin. 2013; 63:11–30. [PubMed: 23335087]
2. Montgomery RB, Mostaghel EA, Vessella R, et al. Maintenance of intratumoral androgens in metastatic prostate cancer: a mechanism for castration-resistant tumor growth. Cancer Res. 2008; 68:4447–4454. [PubMed: 18519708]
3. Bubendorf L, Schopfer A, Wagner U, et al. Metastatic patterns of prostate cancer: an autopsy study of 1,589 patients. Hum Pathol. 2000; 31:578–583. [PubMed: 10836297]
4. Scher HI, Halabi S, Tannock I, et al. Design and end points of clinical trials for patients with progressive prostate cancer and castrate levels of testosterone: recommendations of the Prostate Cancer Clinical Trials Working Group. J Clin Oncol. 2008; 26:1148–1159. [PubMed: 18309951]
5. Morisson C, Jeraj R, Liu G. Imaging of castration-resistant prostrate cancer: development of imaging response biomarkers. Curr Opin Urol. 2013; 23:230–236. [PubMed: 23422587]
6. Ido T, Wan CN, Casella V, et al. Labeled 2-Deoxy-D-Glucose Analogs - F-18-Labeled 2-Deoxy-2-Fluoro-D-Glucose, 2-Deoxy-2-Fluoro-D-Mannose and C-14-2-Deoxy-2-Fluoro-D Glucose. J Labelled Compd Rad. 1978; 14:175–183.
7. Morris MJ, Akhurst T, Larson SM, et al. Fluorodeoxyglucose positron emission tomography as an outcome measure for castrate metastatic prostate cancer treated with antimicrotubule chemotherapy. Clin Cancer Res. 2005; 11:3210–3216. [PubMed: 15867215]
8. Yu EY, Muzi M, Hackenbracht JA, et al. C11-acetate and F-18 FDG PET for men with prostate cancer bone metastases: relative findings and response to therapy. Clin Nucl Med. 2011; 36:192–198. [PubMed: 21285676]
9. Jadvar H. Imaging evaluation of prostate cancer with 18F-fluorodeoxyglucose PET/CT: utility and limitations. Eur J Nucl Med Mol Imaging. 2013; 40:S5–10. [PubMed: 23429934]
10. Meirelles GS, Schoder H, Ravizzini GC, et al. Prognostic value of baseline [18F] fluorodeoxyglucose positron emission tomography and 99mTc-MDP bone scan in progressing metastatic prostate cancer. Clin Cancer Res. 2010; 16:6093–6099. [PubMed: 20975102]
11. Blau M, Nagler W, Bender MA. Fluorine-18: a new isotope for bone scanning. J Nucl Med. 1962; 3:332–334. [PubMed: 13869926]
12. Even-Sapir E, Metser U, Mishani E, Lievshitz G, Lerman H, Leibovitch I. The detection of bone metastases in patients with high-risk prostate cancer: 99mTc-MDP Planar bone scintigraphy, single- and multi-field-of-view SPECT, 18F-fluoride PET, and 18F-fluoride PET/CT. J Nucl Med. 2006; 47:287–297. [PubMed: 16455635]
13. Cook G Jr. Parker C, Chua S, Johnson B, Aksnes AK, Lewington VJ. 18F-fluoride PET: changes in uptake as a method to assess response in bone metastases from castrate-resistant prostate cancer patients treated with 223Ra-chloride (Alpharadin). EJNMMI Res. 2011; 1:4–9. [PubMed: 22214491]
14. Damle NA, Bal C, Bandopadhyaya GP, et al. The role of 18F-fluoride PET-CT in the detection of bone metastases in patients with breast, lung and prostate carcinoma: a comparison with FDG PET/CT and 99mTc-MDP bone scan. Jpn J Radiol. 2013; 31:262–269. [PubMed: 23377765]

15. Hsu WK, Virk MS, Feeley BT, Stout DB, Chatziioannou AF, Lieberman JR. Characterization of osteolytic, osteoblastic, and mixed lesions in a prostate cancer mouse model using 18F-FDG and 18F-fluoride PET/CT. J Nucl Med. 2008; 49:414–421. [PubMed: 18287261]

16. Iagaru A, Mittra E, Yaghoubi SS, et al. Novel strategy for a cocktail 18F-fluoride and 18F-FDG PET/CT scan for evaluation of malignancy: results of the pilot-phase study. J Nucl Med. 2009; 50:501–505. [PubMed: 19289439]

17. Kruger S, Buck AK, Mottaghy FM, et al. Detection of bone metastases in patients with lung cancer: 99mTc-MDP planar bone scintigraphy, 18F-fluoride PET or 18F-FDG PET/CT. Eur J Nucl Med Mol Imaging. 2009; 36:1807–1812. [PubMed: 19504092]

18. Iagaru A, Mittra E, Dick DW, Gambhir SS. Prospective evaluation of (99m)Tc MDP scintigraphy, (18)F NaF PET/CT, and (18)F FDG PET/CT for detection of skeletal metastases. Mol Imaging Biol. 2012; 14:252–259. [PubMed: 21479710]

19. Jadvar H, Desai B, Ji L, et al. Prospective evaluation of 18F-NaF and 18F-FDG PET/CT in detection of occult metastatic disease in biochemical recurrence of prostate cancer. Clin Nucl Med. 2012; 37:637–643. [PubMed: 22691503]

20. Lin FI, Rao JE, Mittra ES, et al. Prospective comparison of combined 18F-FDG and 18F NaF PET/CT vs. 18F-FDG PET/CT imaging for detection of malignancy. Eur J Nucl Med Mol Imaging. 2012; 39:262–270. [PubMed: 22065013]

21. Iagaru A, Mittra E, Mosci C, et al. Combined 18F-fluoride and 18F-FDG PET/CT scanning for evaluation of malignancy: results of an international multicenter trial. J Nucl Med. 2013; 54:176–183. [PubMed: 23243299]

22. Hawkins RA, Choi Y, Huang SC, et al. Evaluation of the skeletal kinetics of fluorine-18-fluoride ion with PET. J Nucl Med. 1992; 33:633–642. [PubMed: 1569473]

23. Doot RK, Muzi M, Peterson LM, et al. Kinetic analysis of 18F-fluoride PET images of breast cancer bone metastases. J Nucl Med. 2010; 51:521–527. [PubMed: 20237040]

24. Sokoloff L, Reivich M, Kennedy C, et al. The [14C]deoxyglucose method for the measurement of local cerebral glucose utilization: theory, procedure, and normal values in the conscious and anesthetized albino rat. J Neurochem. 1977; 28:897–916. [PubMed: 864466]

25. Gambhir SS, Schwaiger M, Huang SC, et al. Simple noninvasive quantification method for measuring myocardial glucose utilization in humans employing positron emission tomography and fluorine-18 deoxyglucose. J Nucl Med. 1989; 30:359–366. [PubMed: 2786939]

26. Fizazi KS, Higano CS, Nelson JB, et al. Phase III, randomized, placebo-controlled study of docetaxel in combination with zibotentan in patients with metastatic castration-resistant prostate cancer. J Clin Oncol. 2013; 31:1740–1747. [PubMed: 23569308]

27. Dehdashti F, Flanagan FL, Mortimer JE, Katzenellenbogen JA, Welch MJ, Siegel BA. Positron emission tomographic assessment of “metabolic flare” to predict response of metastatic breast cancer to antiestrogen therapy. Eur J Nucl Med. 1999; 26:51–56. [PubMed: 9933662]

28. Coleman RE, Mashiter G, Whitaker KB, Moss DW, Rubens RD, Fogelman I. Bone scan flare predicts successful systemic therapy for bone metastases. J Nucl Med. 1988; 29:1354–1359. [PubMed: 3261330]

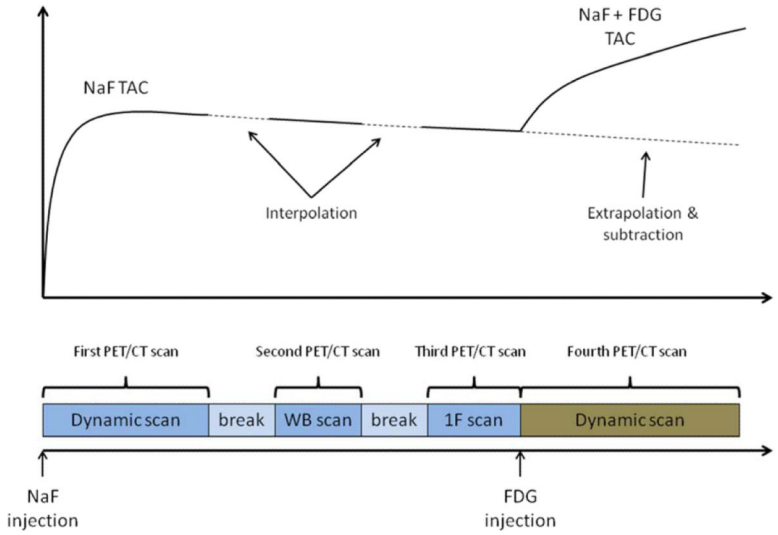

Figure 1.

Schematic representation of the combined NaF/FDG PET/CT image acquisition. Dynamic NaF PET/CT image was constructed from coregistered first PET/CT scan (dynamic scan over one 15 cm segment), second PET/CT scan (whole-body scan) and third PET/CT scan (one-frame scan over 15 cm segment). Dynamic FDG PET/CT scan was constructed by subtracting the NaF baseline activity (obtained by extrapolating the dynamic NaF PET/CT scan) from the fourth PET/CT scan.

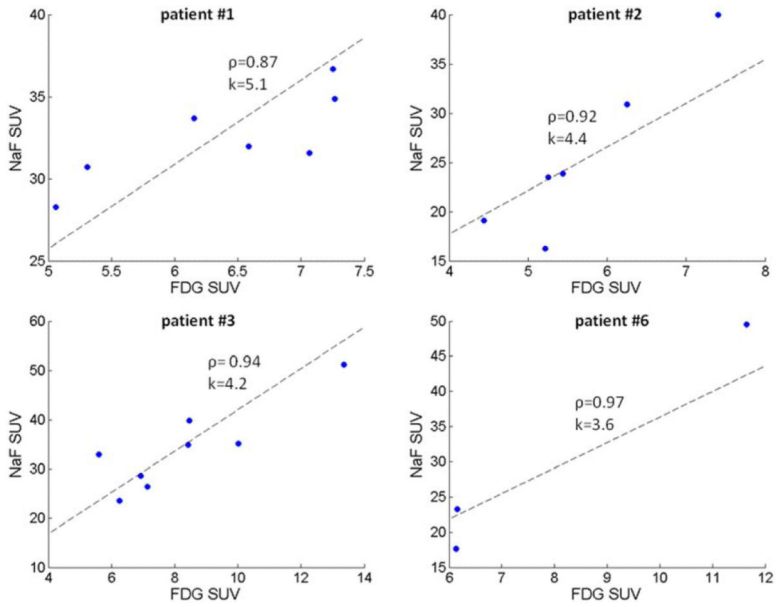

Figure 2.

Correlation plots for NaF and FDG peak SUV. Each graph is for all the lesions of single patients; four patients had multiple lesions in the FOV. Graphs have added correlation coefficient (ρ) and slope of plotted line that was determined as the average ratio of NaF:FDG SUV.

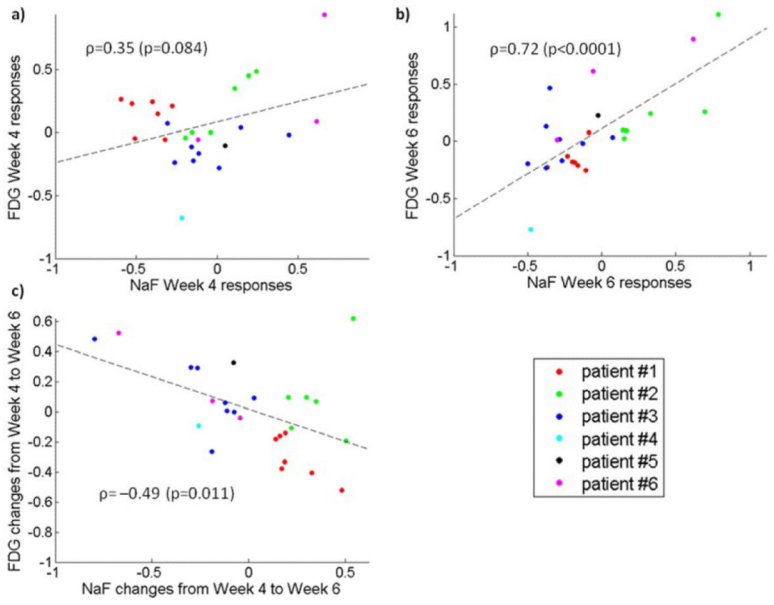

Figure 3.

Correlation plot of NaF and FDG K_i responses. Figure presents NaF versus FDG Week 4 K_i responses (a), NaF versus FDG Week 6 K_i responses (b), and NaF versus FDG K_i changes from Week 4 to Week 6 (c).

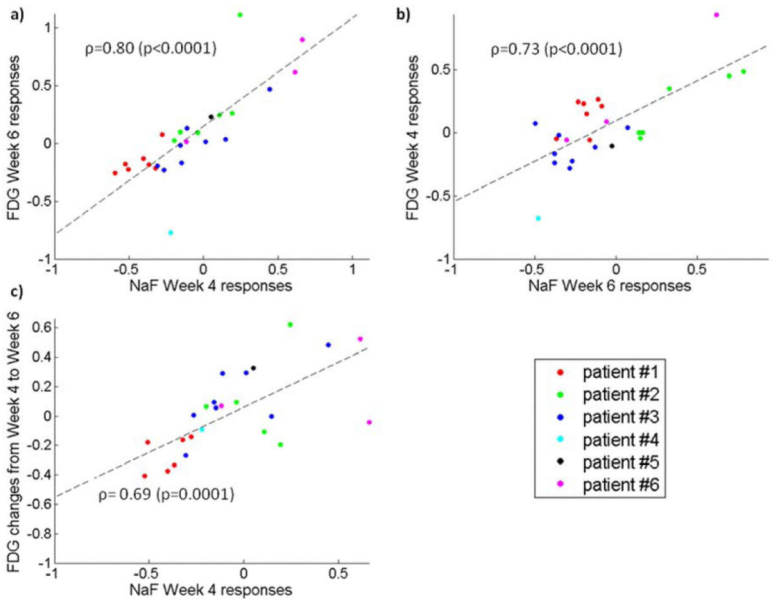

Figure 4.

Correlation plot of non-equivalent NaF and FDG K_i responses. Figure presents NaF Week 4 $K_i$responses versus FDG Week 6 K_i responses (a), NaF Week 6 K_i responses versus FDG Week 4 K_i responses (b), NaF Week 4 K_i responses versus FDG changes from Week 4 to Week 6 (c).

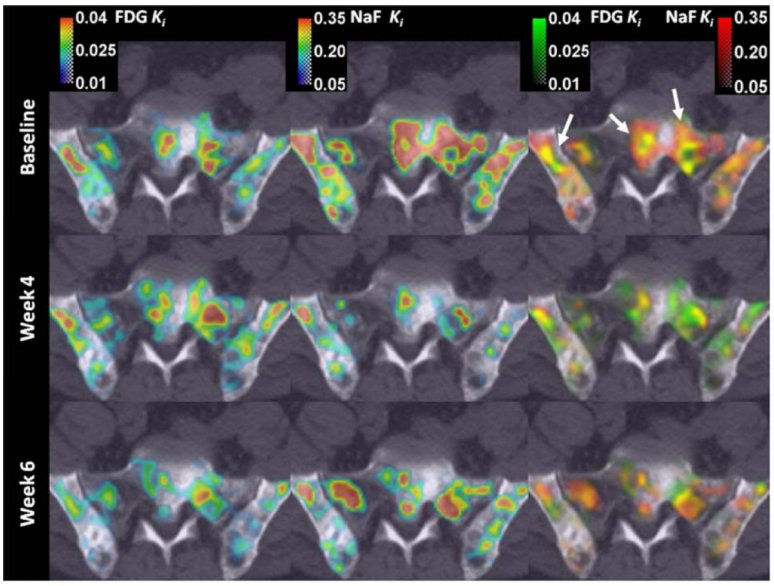

Figure 5.

An example of NaF, FDG and combined K_i parametric images, where the areas of high NaF and high FDG uptakes were notably dislocated. Arrows point on the lesions with most notable dislocation between the NaF and FDG uptake.

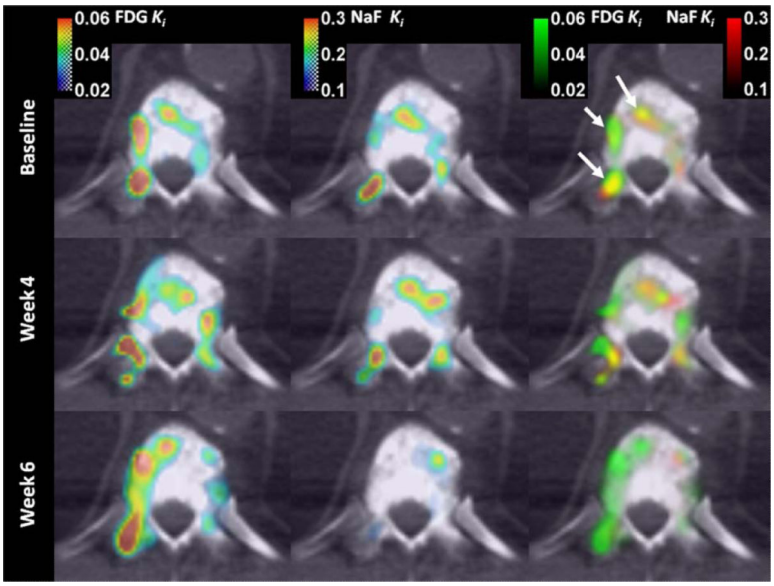

Figure 6.

An example of NaF, FDG and combined K_i parametric images, where the areas of high NaF and high FDG uptakes were less dislocated. Arrows point on the visible lesions with the concordant NaF and FDG uptake.

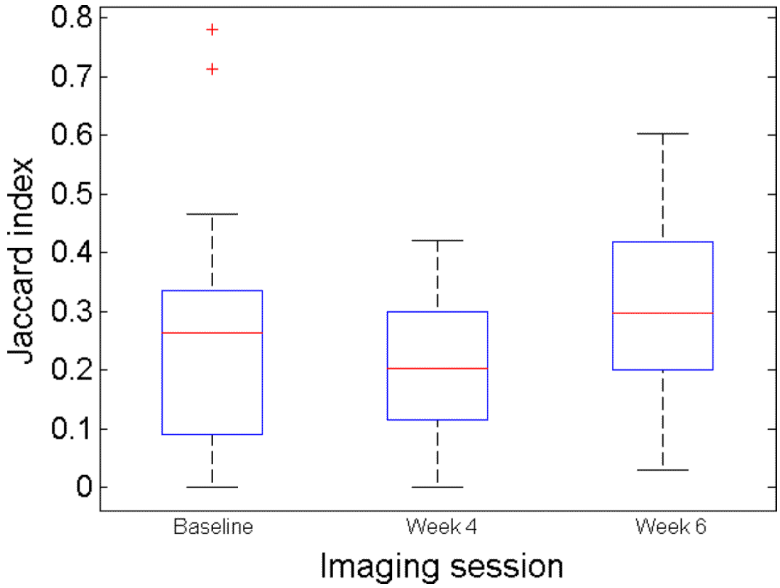

Figure 7.

The concordance of NaF and FDG segmentations for the investigated metastases through the course of therapy.

Table 1

Mean (standard deviation) of peak values of vasculature parameters (K_1, V_b), uptake rate parameter K_i and SUV for both tracers and all imaging sessions, averaged over all segmented lesions.

	NaF peak value			FDG peak value		
	Baseline	**Week 4**	**Week 6**	**Baseline**	**Week 4**	**Week 6**
K_1	0.43 (0.18)	0.48 (0.19)	0.41 (0.17)	0.27 (0.11)	0.35 (0.20)	0.30 (0.15)
V_b	0.15 (0.11)	0.20 (0.16)	0.14 (0.13)	0.22 (0.083)	0.20 (0.072)	0.19 (0.078)
K_i	0.29 (0.17)	0.24 (0.14)	0.25 (0.14)	0.039 (0.019)	0.038 (0.015)	0.039 (0.021)
SUV	33.3 (14.3)	31.2 (13.6)	30.5 (12.1)	7.6 (2.9)	7.0 (2.5)	7.6 (3.5)

Table 2

Mean (standard deviation) of responses obtained from peak values of vasculature parameters (K_1, V_b), uptake rate parameter K_i and SUV. Responses are for both tracers and all imaging sessions, averaged over all segmented lesions.

	NaF response			FDG response		
	Week 4	**Week 6**	**Change Wk4-Wk6**	**Week 4**	**Week 6**	**Change Wk4-Wk6**
K_1	0.12 (0.22)	−0.016 (0.22)	−0.14 (0.23)	0.29 (0.45)	0.15 (0.36)	−0.15 (0.34)
V_b	0.46 (0.59)	0.032 (0.51)	−0.43 (0.60)	−0.023 (0.30)	−0.018 (0.42)	0.0052 (0.32)
K_i	−0.086 (0.33)	−0.058 (0.35)	0.027 (0.33)	0.058 (0.30)	0.065 (0.38)	0.0076 (0.29)
SUV	−0.040 (0.18)	−0.057 (0.18)	−0.019 (0.16)	−0.042 (0.29)	0.031 (0.33)	0.072 (0.26)

Table 3

Correlation coefficients (p-values) of NaF and FDG peak values for Baseline, Week 4 and Week 6 imaging, and responses evaluated at Week 4, Week 6 and Change Wk4-Wk6. All values and responses were evaluated with vasculature parameters (K_1, V_b), uptake rate parameter K_i and SUV. Correlation coefficients are calculated over all segmented lesions.

	Imaging sessions			**Responses**		
	Baseline	**Week 4**	**Week 6**	**Week 4**	**Week 6**	**Change Wk4-Wk6**
K_1	0.62 (0.0007)	0.61 (0.0009)	**0.79 (<0.0001)**	0.31 (0.13)	0.34 (0.085)	0.27 (0.18)
V_b	**0.75 (<0.0001)**	**0.77 (<0.0001)**	**0.81 (<0.0001)**	−0.03 (0.90)	0.10 (0.63)	0.23 (0.26)
K_i	0.61 (0.0009)	**0.76 (<0.0001)**	0.57 (0.0024)	0.35 (0.084)	**0.72 (<0.0001)**	−0.49 (0.011)
SUV	**0.88 (<0.0001)**	0.59 (0.0015)	**0.77 (<0.0001)**	0.35 (0.079)	0.55 (0.0033)	−0.27 (0.18)